LABORATORY INVESTIGATION

MR Coagulation: A Novel Minimally Invasive Approach to Aneurysm Repair

Ouri Cohen, PhD, Ming Zhao, PhD, Erez Nevo, MD, DSc, and Jerome L. Ackerman, PhD

ABSTRACT

Purpose: To demonstrate a proof of concept of magnetic resonance (MR) coagulation, in which MR imaging scanner–induced radiofrequency (RF) heating at the end of an intracatheter long wire heats and coagulates a protein solution to effect a vascular repair by embolization.

Materials and Methods: MR coagulation was simulated by finite-element modeling of electromagnetic fields and specific absorption rate (SAR) in a phantom. A glass phantom consisting of a spherical cavity joined to the side of a tube was incorporated into a flow system to simulate an aneurysm and flowing blood with velocities of 0–1.7 mL/s. A double-lumen catheter containing the wire and fiberoptic temperature sensor in 1 lumen was passed through the flow system into the aneurysm, and 9 cm^3 of protein solution was injected into the aneurysm through the second lumen. The distal end of the wire was laid on the patient table as an antenna to couple RF from the body coil or was connected to a separate tuned RF pickup coil. A high RF duty-cycle turbo spin-echo pulse sequence excited the wire such that RF energy deposited at the tip of the wire coagulated the protein solution, embolizing the aneurysm.

Results: The protein coagulation temperature of 60°C was reached in the aneurysm in ~12 seconds, yielding a coagulated mass that largely filled the aneurysm. The heating rate was controlled by adjusting pulse-sequence parameters.

Conclusions: MR coagulation has the potential to embolize vascular defects by coagulating a protein solution delivered by catheter using MR imaging scanner–induced RF heating of an intracatheter wire.

ABBREVIATIONS

HSA = human serum albumin, MT = magnetization transfer, RF = radiofrequency, SAH = subarachnoid hemorrhage, SAR = specific absorption rate

Intracranial aneurysms occur in an estimated 1%–6% of the population (1), with the most common presentation being subarachnoid hemorrhage (SAH) (2). Current treatment methods consist of (*i*) microvascular neurosurgical clipping (3); (*ii*) endovascular coil embolization (4), which may be combined with temporary caging for wide-necked aneurysms (5); and (*iii*) embolization with the use of a coagulable material such as Onyx (Micro Therapeutics, Irvine, California) (6) or recently developed polymeric foams (7). Neurosurgical clipping is highly invasive because it entails clipping the aneurysm at its base via an open surgical approach to prevent rupture. Additionally, in clinical trials, clipping presents less favorable outcomes than coil embolization (8,9). Although it is minimally invasive, a disadvantage of coil embolization is a possible reopening of the aneurysm that may be caused by impaction of the coils (8). Finally, embolization with coagulable materials yields improved packing compared with coil embolization but requires the injection of possibly immunogenic foreign materials.

The present study describes a novel minimally invasive embolization method, magnetic resonance (MR) coagulation, that does not require the permanent implantation of artificial objects (eg, coils) or foreign materials (eg, Onyx, polymeric foams) to achieve embolization, and does not necessarily require temporary occlusion of normal blood flow. Instead, a biomaterial that can be coagulated by mild

From the Athinoula A. Martinos Center for Biomedical Imaging, Department of Radiology (O.C., M.Z., J.L.A.), Massachusetts General Hospital, Charlestown, Massachusetts; Department of Radiology (O.C., J.L.A.), Harvard Medical School, Boston, Massachusetts; Department of Physics and Applied Physics (M.Z.), University of Massachusetts Lowell, Lowell, Massachusetts; and Robin Medical Inc. (E.N.), Baltimore, Maryland. Received March 20, 2017; final revision received June 21, 2017; accepted June 27, 2017. **Address correspondence to** O.C., Athinoula A. Martinos Center for Biomedical Imaging, Room 2301, Department of Radiology, Massachusetts General Hospital, 149 13th St., Charlestown, MA 02129; E-mail: ouri@nmr.mgh.harvard.edu

E.N. is an employee of Robin Medical Inc. (Baltimore, Maryland). None of the other authors have identified a conflict of interest.

http://dx.doi.org/10.1016/j.jvir.2017.06.036

heating is injected into the aneurysm and coagulated by using the heat generated by the MR imaging scanner. The scanner also provides the necessary intraprocedural image guidance and assesses the efficacy of the repair. The MR imaging scanner permits fine control and real-time monitoring of the coagulation process and significantly simplifies the embolization procedure.

In this report, egg white, a conveniently available protein solution, is used as the biomaterial. In clinical practice, the use of a more human-compatible material such as human serum albumin (HSA), a naturally present blood protein that is nonthrombogenic and nonimmunogenic, is envisioned. The MR coagulation concept is illustrated in **Figure 1**. The potential of MR coagulation is demonstrated via electromagnetic simulations and phantom experiments that mimic typical conditions encountered in in vivo aneurysms.

MATERIALS AND METHODS

Electromagnetic Simulation and Model Description

The feasibility of the proposed technique for directing RF energy from the scanner's body RF coil to the aneurysm was tested by numeric simulation of two device configurations using an electromagnetic finite-element solver (HFSS; Ansys, Canonsburg, Pennsylvania). In one device configuration, a standalone wire was used to harvest the RF energy from the scanner. The standalone wire was a polytetrafluoroethylene-insulated 24-gauge (American wire gauge) wire with 0.5 cm exposed at the tip. In the second configuration, an RF coil tuned to the scanner's Larmor frequency was used in conjunction with the wire. The aneurysm was modeled as a 15-mm-diameter sphere. The sphere's dielectric properties were set to those of blood (10,11).

Phantom, Flow, and Catheter System

A spherical glass aneurysm phantom with a 15-mm outside diameter was manufactured (Yankee Glassblower, Concord, Massachusetts). A glass phantom was chosen because it is made of an MR-compatible material, is easily shaped, and allows visualization of the coagulum. The smoothness of the glass walls ensured that successful adhesion of the coagulum in vitro would be successful in vivo as well. A peristaltic pump (Cole-Parmer, Vernon Hills, Illinois) provided a controllable pulsatile saline solution flow through the phantom. Hemostatic Y-valves permitted the insertion of a DuraFlow 14-F double-lumen catheter (AngioDynamics, Latham, New York) while preventing the introduction of air bubbles into the system. A 26-gauge Teflon-insulated silver-plated solid copper wire (Alpha Wire, Elizabeth, New Jersey) was connected to a 30-cm × 30-cm square RF loop coil tuned to the Larmor frequency. The RF loop coil was placed against the scanner's inner bore. The other end of the wire and a Luxtron fiberoptic temperature sensor (LumaSense Technologies, Santa Clara, California) were inserted into one lumen of the catheter and positioned such that the wire and sensor tips emerged by approximately 5 mm from the catheter tip. The catheter assembly was guided into the aneurysm. Temperatures were sampled at 1-s intervals.

Chicken egg white, a low-cost protein solution source, was used as the coagulable biomaterial. Ovalbumin, a protein with coagulation properties similar to those of HSA, is the major protein constituent in egg white.

MR Imaging and MR Coagulation

Experiments were carried out in an Avanto 1.5-T scanner (Siemens, Erlangen, Germany) by using its built-in body RF coil for RF excitation. A high RF duty cycle turbo spin-echo

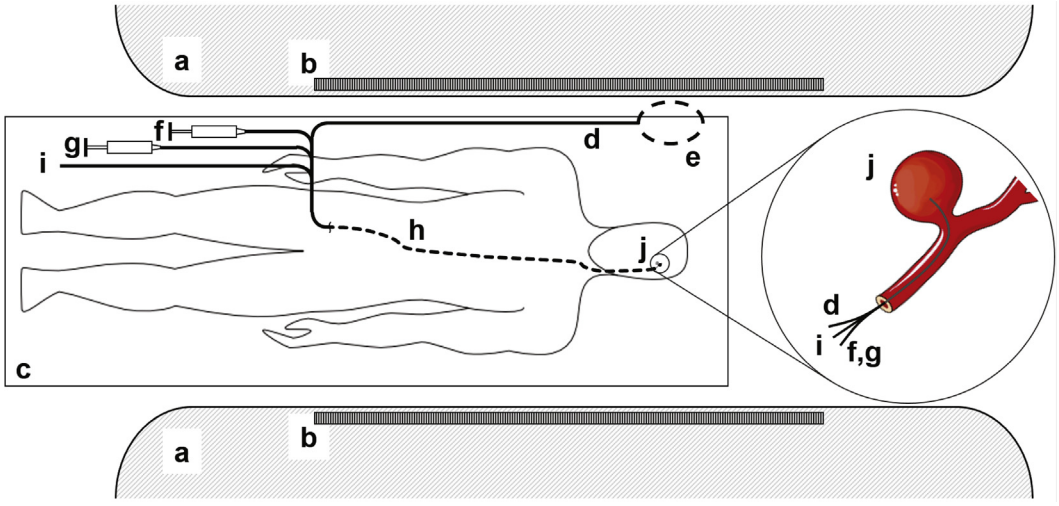

Figure 1. MR coagulation concept: (*a*) MR imaging scanner magnet assembly, (*b*) body RF coil, and (*c*) patient table. (*d*) Long wire RF pickup antenna is magnetically coupled to the body coil; RF pickup may be optionally enhanced with a tuned RF pickup loop (*e*) connected to the free end of the wire. (*f*) Protein solution and (*g*) saline solution for flushing share one lumen of the catheter (*h*) inserted percutaneously into the femoral aorta. (*i*) Fiberoptic temperature sensor shares the second lumen of catheter with the wire. (*j*) Cerebral aneurysm.

sequence provided the necessary RF heating. The field of view was set to 300 mm × 300 mm with a matrix size of 128 × 128 and a slice thickness of 5 mm. With the repetition time set to 300 ms, the total scan duration (ie, heating time) was 2 min. Tuning and detuning the attached RF coil enabled general control over the heating, whereas adjusting the repetition time permitted fine control of the RF duty cycle.

RESULTS

Electromagnetic Simulation

Figure 2 shows the specific absorption rate (SAR) in the aneurysm computed by the simulations on a log scale. Both configurations exhibited increased SAR near the wire tip. However, the maximum SAR for the coil configuration was approximately 40-fold higher than the standalone wire configuration, reaching a maximum of ~80 W/kg in contrast to the ~2 W/kg attained by the wire configuration. In both cases the SAR increase was highly localized to the wire tip in the aneurysm (Fig 3), mitigating potential concerns about unintended heating of neighboring tissues.

Saline Solution Heating

The heating was initially measured without flow to ensure that the proposed device could provide sufficient heating for coagulation. The coil configuration yielded the greatest heating and allowed simple control of the heating rate by tuning or detuning the resonant circuit comprising the RF coil, and was therefore used for all subsequent experiments. The heating sequence was applied for 30 s, and the temperature increase was recorded throughout the experiment with the fiberoptic thermometer. As predicted by a simple heat-transfer model of the aneurysm in contact with an infinite heat sink (equivalent to the surrounding tissue remaining at fixed temperature), the temperature increased during heating at a fixed duty cycle to asymptotically approach a maximum temperature and decreased exponentially toward the baseline temperature when the sequence was turned off (Fig 4). By using the pulse sequence parameters described earlier, the temperature increased at a rate of ~2–3°C/s, reaching the ~60°C needed to coagulate the protein solution in ~12 s.

Effect of Flow on Heating Rate

Thermal bioregulation mechanisms including blood flow help dissipate heat in tissues, which can affect the maximum temperature achievable in vivo. The effect of different flow rates on the achievable temperature increase was therefore studied. The heating experiment was repeated multiple times for flow rates in the range of 0–1.7 mL/s, and the

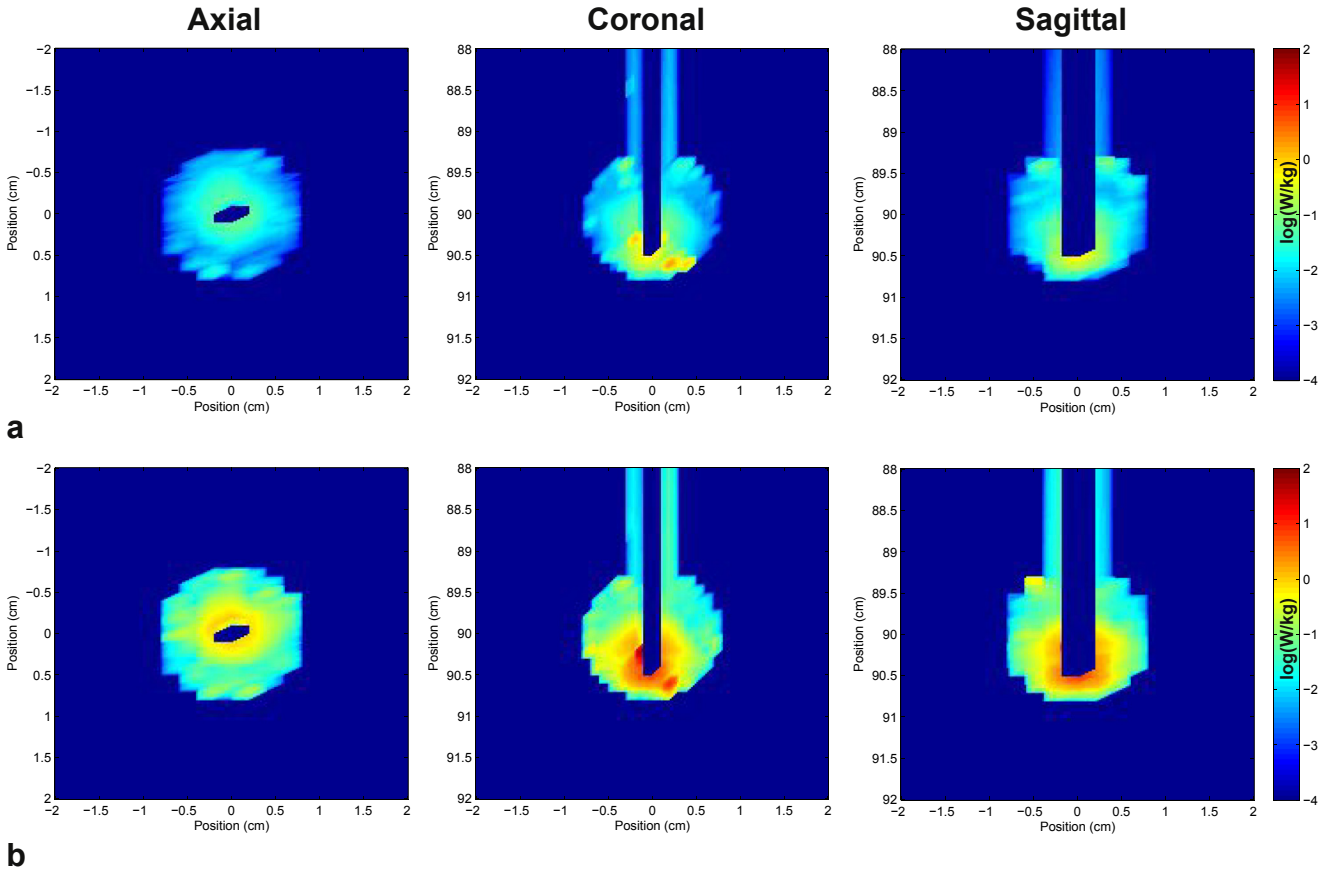

Figure 2. Axial, coronal, and sagittal maps of the local SAR on a log scale for the simulated standalone wire **(a)** and coil **(b)** configurations of the proposed device. Although both configurations showed increases in the SAR, the SAR for the coil configuration was ~40 fold greater.

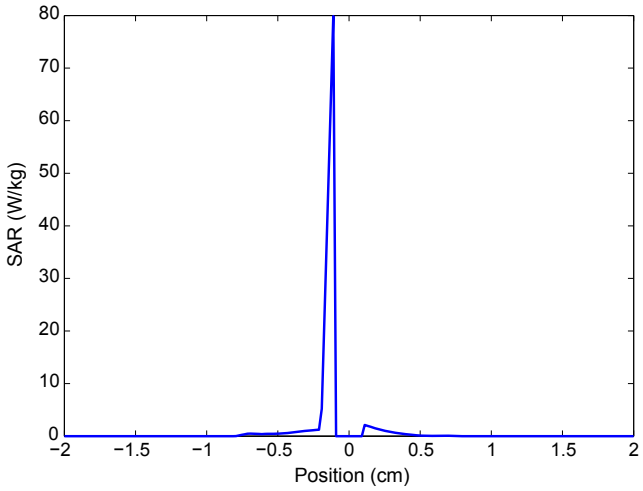

Figure 3. Local SAR as a function of position for the coil configuration of the device. Note that, despite the large SAR attained in proximity to the wire, the heating is highly localized and therefore unlikely to adversely impact neighboring tissues.

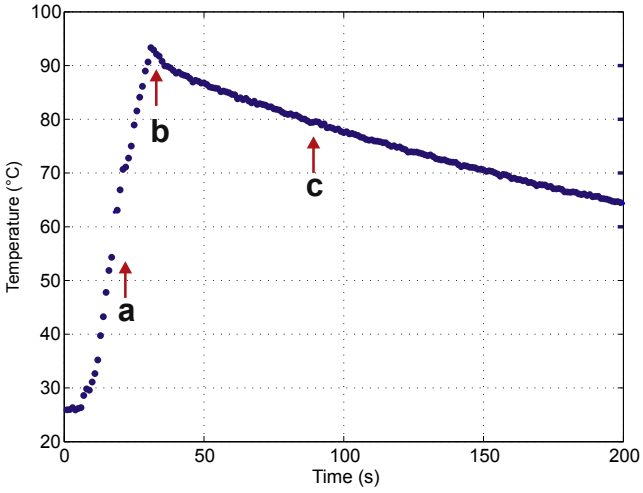

Figure 4. Temperature measured while the heating pulse sequence was activated (*a*). The temperature increased exponentially until the pulse sequence was turned off (*b*) and then decreased exponentially as well (*c*). The high temperatures achieved were significantly greater than the ~60°C needed for protein coagulation.

temperature increase in the aneurysm was measured. This range of flow rates is representative of different clinical paradigms in aneurysm repair, with a flow rate of 0 mL/s being equivalent to a balloon-assisted embolization (12), whereas 0.5 mL/s is the flow rate past cerebral aneurysms in small vessels (13) with unobstructed blood flow. The heating rate (ie, initial slope of the temperature-vs-time curve) for each experiment was calculated by fitting the temperature T as a function of time t to the equation $T = A - B \cdot \exp(-t/C)$ using the Levenberg–Marquardt algorithm (14), with A, B, and C adjustable parameters.

The relationship between the heating rates and the corresponding flow rates was determined by a linear least-squares

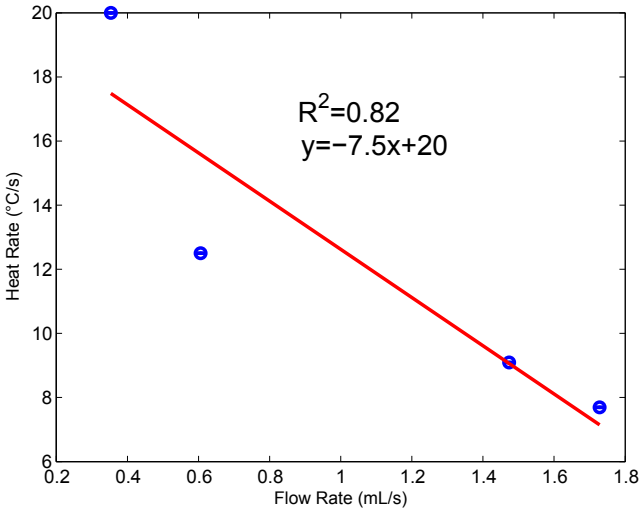

Figure 5. Heating rate as a function of the saline solution flow rate. Increased flow rate caused a faster heat exchange between the inflowing room-temperature saline solution and the saline solution in the aneurysm, resulting in a lower rate of temperature increase within the aneurysm.

fitting of the data. Although increased flow resulted in lower heating rates (as a result of increased heat transport out of the aneurysm by flowing saline solution), heating was nevertheless sufficient for coagulation even at the highest flow rate tested (Fig 5).

Coagulation

The heating pulse sequence was activated with the flow rate set to 0.5 mL/s to simulate an unobstructed embolization procedure. The temperature was allowed to increase unperturbed for ~15 s to exceed the 60°C needed for coagulation. When the temperature reached ~80°C, 6 cm^3 of egg white was injected into the catheter. As the egg white was initially at room temperature, its injection caused a temporary decrease in temperature, so the temperature was allowed to recover to greater than 60°C before injection of the remaining 3 cm^3 of egg white (Fig 6, left). In total, 9 cm^3 of egg white was injected into the catheter to ensure that the resulting coagulum would fill a significant portion of the aneurysm to facilitate visualization. This quantity of injected protein solution also dictated the ~2-min total heating time to ensure full coagulation. The resulting coagulum, shown in the right panel of Figure 6, was densely packed around the heating wire with no coagulum present in the adjoining tubes, indicating good adhesion to the aneurysm walls.

Real-Time Monitoring of Coagulation

The egg white magnetic relaxation properties change progressively as a result of the coagulation and therefore provide a means of tracking the state of the coagulation. Because magnetization transfer (MT) imaging (15) provides the greatest contrast between coagulated and uncoagulated albumin protein, it was used to monitor progression of

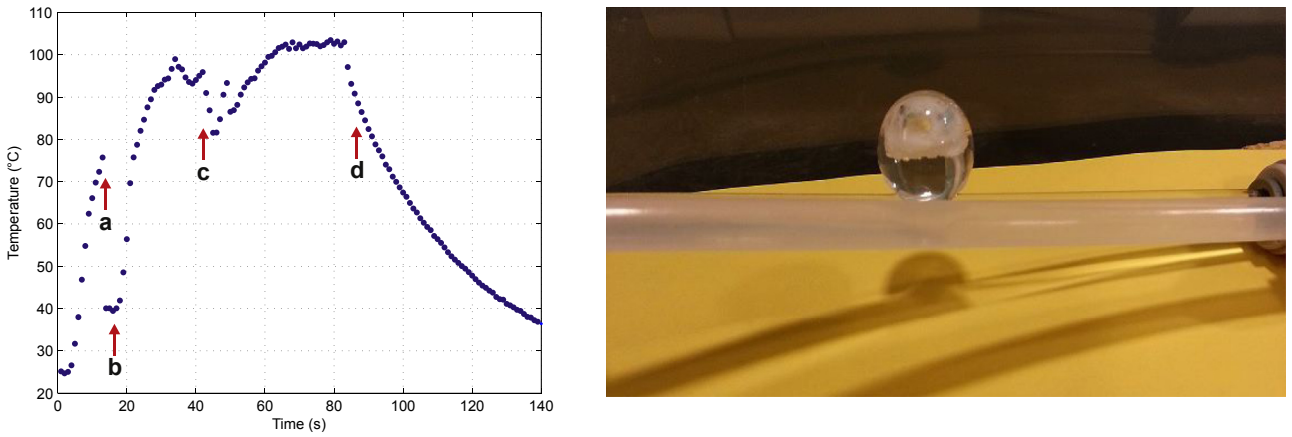

Figure 6. Temperature profile for a coagulation experiment under flow (left). The room-temperature egg white injected when the temperature reached ~75°C (*a*) caused a temporary decrease in the measured temperature (*b*). A second egg-white bolus was injected after allowing the temperature to recover back to its previous level (*c*). The heating pulse sequence was turned off after 80 s, and the sample was allowed to cool (*d*). The resulting coagulum in the aneurysm (right) demonstrates that, despite the significant flow and smoothness of the glass walls, the coagulated albumin nevertheless adhered to the aneurysm.

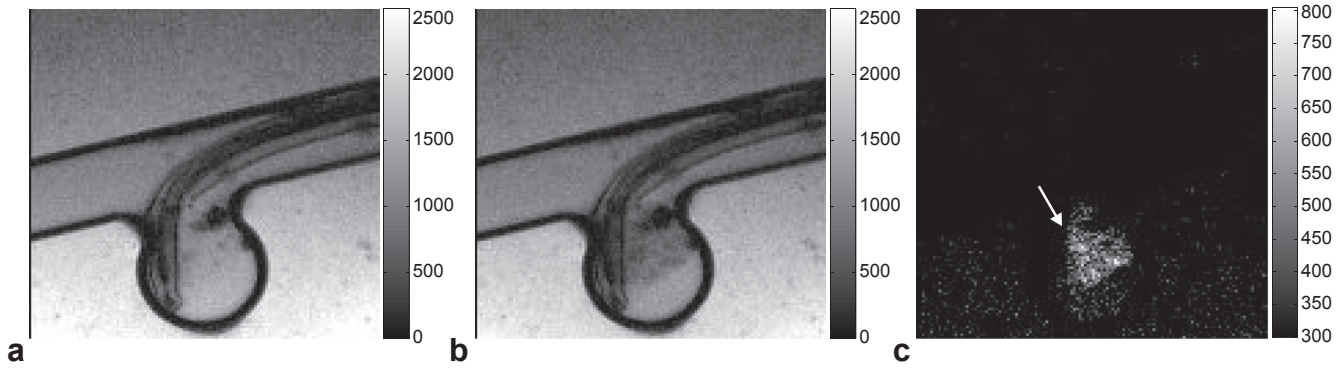

Figure 7. MT images acquired before **(a)** and after **(b)** coagulation. The hyperintense regions in the image showing the difference (arrow, **c**) indicate the location and morphology of the coagulum. MT MR imaging enables intraprocedural monitoring of the progress of coagulation.

coagulation. MT images before and after coagulation (**Fig 7**) illustrate the feasibility of intraprocedural monitoring of the coagulation process.

DISCUSSION

In the present study, MR-mediated RF ablation (16), a recently introduced method that harnesses the energy generated by the scanner for use in RF ablation, was adopted for heating a coagulable material (ie, protein solution) to embolize a vascular defect. The method does not require an external RF power generator or electrical connections to any external system, avoiding the need for a grounding pad to complete the electrical path and eliminating the possibility of accidental skin burns (17–19) caused by poor contact of the grounding pad (20). The RF energy generated by the MR scanner is focused by using a passive conductive device (eg, a wire) to obtain localized heating. Unlike the present study, previous studies (21,22) of RF-induced heating relied on custom RF coils and necessitated the use of ionizing imaging modalities for treatment monitoring.

Minimally invasive vascular embolization methods reduce recovery times and yield better clinical outcomes compared with surgical clipping (8,9). Nevertheless, given their use of foreign agents or materials, current embolization methods are susceptible to an immune response as well as inflammation, which can be severe in some cases (23,24). In contrast, HSA is a nonthrombogenic and nonimmunogenic protein naturally found in human blood plasma. These properties, along with a low temperature of coagulation (50°C–60°C) render it attractive for in vivo use.

In the present study, the hypothesis that MR RF heating can be used to successfully occlude an aneurysm by coagulation of an injected protein solution was tested by using egg white as an inexpensive substitute for HSA. The findings (**Figs 6**, **7**) support this hypothesis.

Temperatures approaching 100°C were achieved in seconds despite a flow of cooler room-temperature saline solution. As protein solutions begin to coagulate at temperatures of approximately 60°C, the temperatures achieved in these experiments are more than sufficient to coagulate the protein on contact, as demonstrated in **Figure 6**.

The equilibrium temperature reached depended on the sequence parameters (ie, pulse amplitude, duty cycle, flip angle) as well as the saline solution flow rate. However, following coagulation, increasing the flow rate had minimal impact on the temperature within the aneurysm, indicating the effectiveness of the coagulum at halting the flow inside the aneurysm.

Alternative embolization methods occasionally rely on balloon-assisted techniques to facilitate coagulation by restricting blood flow past or into the aneurysm, albeit at the cost of undesirable arterial blood flow reduction (25). Because inadequate blood perfusion can cause irreversible tissue damage in minutes (26), procedure durations must be strictly limited to avoid the damage caused by cerebral hypoperfusion. Additionally, in some cases (12), the tortuosity of brain vessels may prohibit the use of balloons altogether. In contrast, the method proposed here allows coagulation in narrow-necked aneurysms under normal flow and could therefore mitigate the risk of cerebral hypoperfusion and the consequent neurologic damage.

Coagulable materials offer improved packing of the aneurysm and do not depend on the development of occlusive thrombus, and may therefore reduce the rate of recanalization (27,28). Unlike Onyx or more recently introduced polyurethane-based foams that solidify with heating (7), the method proposed here offers the same packing benefits but without the use of potentially immunogenic materials, and, importantly, the treatment can be monitored with MR imaging, a nonionizing imaging modality. Real-time MR guidance is a rapidly developing field, and has been shown to yield improved localization versus fluoroscopy (29). In MR coagulation, catheter guidance is facilitated by the visual artifact induced by the increased local B1 field caused by the heating wire.

A key concern in aneurysm repair is the increased risk of thromboembolic complications following treatment. As shown in **Figure 6**, the albumin coagulated under typical aneurysmal flow conditions adhered to the smooth glass aneurysm walls long after the experiment was terminated and did not flow downstream, reducing the risk of stroke in a clinical setting. It is likely that coagulated albumin will adhere at least as well to aneurysm walls. Nevertheless, an intraluminal filter or balloon can be used to ensure retention of the introduced albumin inside the aneurysm, thereby mitigating any embolization risk.

The present study has a number of limitations. The glass aneurysm phantom is an idealization of the shape of an actual small-necked aneurysm. Glass lacks the surface, mechanical, chemical, and electrical properties of real aneurysms. Adherence of the coagulum to the aneurysmal wall in vivo is likely to be better than its adherence to glass. However, the compliance and continual movement of arterial and aneurysmal walls in vivo could lead to loss of adherence. The electrical behavior of the wire is likely to be different when immersed in an environment with electrical conductivity to the surrounding tissue, rather than in the electrically insulating phantom. The phantom is a large-scale model of the geometry that might be encountered in a real aneurysm. The vessel diameter and the catheter size required in an actual MR coagulation procedure will be much smaller, which may require the use of alternative temperature-monitoring methods (30,31).

The heating curves often display instability as the asymptotic temperature is reached. This is likely the result of unstable flow (eg, convection and turbulence) at the wire tip, boiling or bubble formation, thermal or electrochemical corrosion of the wire tip surface, cycles of buildup and breakthrough of an insulating layer, and similar effects. These can lead to a foamy or flocculent coagulum, which is porous, less coherent, and prone to disintegration. Bubble formation and heating of adjacent tissues are critical safety concerns. Based on the simulation results of **Figure 3** and other RF heating studies conducted on ex vivo liver tissue (16), the heating of adjacent tissues is likely to be minimal. Nevertheless, additional research will be needed to conclusively address these issues.

Subsequent investigations must include varying the protein concentration of the solution. A higher concentration will require less energy to coagulate because less solvent (ie, water) would need to be heated to the coagulation temperature, and the resulting coagulum will have a higher Young modulus (because the coagulum will be less diluted with water). However, a higher concentration results in a more viscous solution, making injection through a long, narrow lumen difficult. Studies that use HSA and studies in animal models of aneurysm will need to be conducted.

It is tempting to envision the use of an interventional guide wire for the conductive wire in MR coagulation. The wire used in this proof-of-concept study was a standard solid copper wire, which exhibits good RF electrical conductivity and is completely nonmagnetic. Stainless steel and Nitinol alloys commonly used in guide wires have much lower electrical conductivity compared with silver or copper, and tend to have high magnetic susceptibility, which introduces image artifacts. Copper and its alloys have high electrical conductivity and magnetic susceptibilities similar to those of water and tissue, and may have the requisite mechanical properties necessary for guide wires. A study of the suitability of different interventional guide wires for MR coagulation is beyond the scope of the present paper and will be examined in future work.

In conclusion, the present study has demonstrated the potential of MR coagulation for the embolization of a vascular defect in a phantom by coagulating a protein solution delivered by catheter using MR imaging scanner–induced RF heating of an intracatheter wire.

ACKNOWLEDGMENTS

We thank R. Gilberto González for help with concept development. Clip art from the Servier Medical Art image bank (*www.servier.com*) was used in **Figure 1**. This research was supported by Center for the Integration of Medicine and Innovative Technology Grant 13-1180/Grant

W81XWH-09-2-001 from US Army Medical Research and Materiel Command and National Institutes of Health Grants RR023009 and P41RR14075.

REFERENCES

1. Wiebers DO. Unruptured intracranial aneurysms: natural history, clinical outcome, and risks of surgical and endovascular treatment. Lancet 2003; 362:103–110.
2. Rinkel GJ, Gijn J, van Wijdicks EF. Subarachnoid hemorrhage without detectable aneurysm. A review of the causes. Stroke 1993; 24: 1403–1409.
3. Thorell W, Rasmussen P, Perl J, Masaryk T, Mayberg M. Balloon-assisted microvascular clipping of paraclinoid aneurysms: technical note. J. Neurosurg 2004; 100:713–716.
4. Brilstra EH, Rinkel GJ, van der Graaf Y, van Rooij WJJ, Algra A. Treatment of intracranial aneurysms by embolization with coils a systematic review. Stroke 1999; 30:470–476.
5. Ito H, Onodera H, Wakui D, et al. The "temporary caging" technique for catheter navigation in patients with intracranial wide-necked aneurysms. Int J Clin Exp Med 2015; 8:11214–11219.
6. Cekirge HS, Saatci I, Ozturk MH, et al. Late angiographic and clinical follow-up results of 100 consecutive aneurysms treated with Onyx reconstruction: largest single-center experience. Neuroradiology 2006; 48:113–126.
7. Rodriguez JN, Clubb FJ, Wilson TS, et al. In vivo response to an implanted shape memory polyurethane foam in a porcine aneurysm model. J Biomed Mater Res A 2014; 102:1231–1242.
8. van der Schaaf I, Algra A, Wermer M, et al. Endovascular coiling versus neurosurgical clipping for patients with aneurysmal subarachnoid haemorrhage. Cochrane Database Syst Rev 1996; 4:CD003085.
9. Molyneux A. International Subarachnoid Aneurysm Trial (ISAT) of neurosurgical clipping versus endovascular coiling in 2143 patients with ruptured intracranial aneurysms: a randomised trial. Lancet 2002; 360: 1267–1274.
10. Gabriel C, Gabriel S, Corthout E. The dielectric properties of biological tissues: I. Literature survey. Phys Med Biol 1996; 41:2231.
11. Hirsch FG, Texter EC, Wood LA, et al. The electrical conductivity of blood I. Relationship to erythrocyte concentration. Blood 1950; 5:1017–1035.
12. Cottier JP, Pasco A, Gallas S, et al. Utility of balloon-assisted Guglielmi detachable coiling in the treatment of 49 cerebral aneurysms: a retrospective, multicenter study. AJNR Am J Neuroradiol 2001; 22:345–351.
13. Levitt MR, McGah PM, Aliseda A, et al. Cerebral aneurysms treated with flow-diverting stents: computational models with intravascular blood flow measurements. AJNR Am J Neuroradiol 2014; 35:143–148.
14. Moré JJ. The Levenberg-Marquardt algorithm: implementation and theory. Numer Analysis 1978; 630:105–116.
15. Wolff SD, Balaban RS. Magnetization transfer imaging: practical aspects and clinical applications. Radiology 1994; 192:593–599.
16. Ackerman JL, Hue YK, Nevo E, et al. MR-mediated radio frequency ablation. In: Program and abstracts from the International Society for Magnetic Resonance in Medicine (ISMRM) 19th Annual Meeting and Exhibition; May 7–13, 2011; Montreal, QC, Canada; p. 1761.
17. Schutt DJ, Haemmerich D. Sequential activation of a segmented ground pad reduces skin heating during radiofrequency tumor ablation: optimization via computational models. IEEE Trans Biomed Eng 2008; 55: 1881–1889.
18. Bleicher RJ, Allegra DP, Nora DT, Wood TF, Foshag LJ, Bilchik AJ. Radiofrequency ablation in 447 complex unresectable liver tumors: lessons learned. Ann Surg Oncol 2003; 10:52–58.
19. Goette A, Reek S, Klein HU, Geller JC. Case report: severe skin burn at the site of the indifferent electrode after radiofrequency catheter ablation of typical atrial flutter. J Interv Card Electrophysiol 2001; 5:337–340.
20. Brace CL, Laeseke PF, Sampson LA, Frey TM, Mukherjee R, Lee FT. Radiofrequency ablation with a high-power generator: device efficacy in an in vivo porcine liver model. Int J Hyperthermia 2007; 23:387–394.
21. Chopra PS, Kandarpa K, Welch WR, Chakrabarti J. Endoluminal thermal occlusion of the ureter with the electromagnetic field-focusing device. J Vasc Interv Radiol 1992; 3:305–312.
22. Kandarpa K, inventor; Brigham and Women's Hospital, assignee. Method and device for recanalization of a body passageway. US Patent 5178618A. January 12, 1993.
23. Duffner F, Ritz R, Bornemann A, Freudenstein D, Wiendl H, Siekmann R. Combined therapy of cerebral arteriovenous malformations: histological differences between a non-adhesive liquid embolic agent and n-butyl 2-cyanoacrylate (NBCA). Clin Neuropathol 2001; 21:13–17.
24. Murayama Y, Viñuela F, Ulhoa A, et al. Nonadhesive liquid embolic agent for cerebral arteriovenous malformations: preliminary histopathological studies in swine rete mirabile. Neurosurgery 1998; 43:1164–1172.
25. Harclerode Z, Andrzejowski J, Coley S, Dyde R. Bispectral index detects intraoperative cerebral ischaemia during balloon assisted cerebral aneurysm coiling. F1000Res 2013; 2:225.
26. Heiss W. Progress in cerebrovascular disease: flow thresholds of functional and morphological damage of brain tissue. Stroke 1983; 14:329–331.
27. Hope JA, Byrne JV, Molyneux AJ. Factors influencing successful angiographic occlusion of aneurysms treated by coil embolization. AJNR Am J Neuroradiol 1999; 20:391–399.
28. Mawad ME, Mawad JK, Cartwright J, Gokaslan Z. Long-term histopathologic changes in canine aneurysms embolized with Guglielmi detachable coils. AJNR Am J Neuroradiol 1995; 16:7–13.
29. Meyer BC, Brost A, Kraitchman DL, et al. Percutaneous punctures with MR imaging guidance: comparison between MR imaging–enhanced fluoroscopic guidance and real-time MR imaging guidance. Radiology 2013; 266:912–919.
30. Poorter JD, Wagter CD, Deene YD, Thomsen C, Stahlberg F, Achten E. Noninvasive MRI thermometry with the proton resonance frequency (PRF) method: in vivo results in human muscle. Magn Reson Med 1995; 33:74–81.
31. Rieke V, Pauly KB. MR thermometry. J Magn Reson Imaging 2008; 27: 376–390.